Fluorescence based Nano Oxygen Particle (FNOP) for Spatiometric Monitoring of Cell Physiological Conditions

Manohar Prasad Koduri[1,6], Venkanagouda S. goudar[2], Yu-Wei Shao[3], John A. Hunt [4,5], James R. Henstock [5], Judith Curran[6], and Fan Gang Tseng[1,2,3,7]**

[1]International Intercollegiate Ph.D. Program, National Tsing Hua University, Taiwan ROC.

[2]Department of Engineering and System Science, Frontier Research Center on Fundamental and Applied Sciences of Matters, National Tsing Hua University, Taiwan ROC.

[3]Institute of Nano Engineering and Microsystems, National Tsing Hua University, Taiwan ROC

[4] School of Science and Technology, Nottingham Trent University, Nottingham NG11 8NS, UK.

[5] Institute of Ageing and Chronic Disease, William Henry Duncan Building, University of Liverpool, Liverpool L7 8TX, UK.

[6] Department of Mechanical, Materials and Aerospace, School of Engineering, University of Liverpool, Harrison Hughes Building, Liverpool, L69 3GH, UK.

[7]Research Center for Applied Sciences, Academia Sinica, Taipei, Taiwan ROC.

Abstract:

Closed-loop artificial pancreas systems have recently been proposed as a solution for treating stage I diabetes by reproducing the function of the pancreas. However, there are many unresolved issues associated with their development, including monitoring and controlling oxygen, immune responses and the optimization of glucose. All of which need to be monitored and controlled to produce an efficient and viable artificial organ, that can become integrated in the patient and maintain homeostasis. This research focused on monitoring oxygen concentration, specifically achieving this kinetically as the oxygen gradient in an artificial pancreas made of alginate spheres containing islet cells. Functional Nanoparticle (NP) for measuring the oxygen gradient in different hydrogel cellular environments using fluorescence-based (F) microscopy were developed and tested. By ester bond, a linker Pluronic F127 was conjugated with a carboxylic acid modified polystyrene Nanoparticle (510 nm). A hydrophilic/ hydrophobic interaction between the commercially available oxygen sensitive fluorophore with F127 results in Fluorescence-based Nano oxygen particle (FNOP). The in-house synthesized FNOP was calibrated inside electro sprayed alginate filled hydrogels and demonstrated a good broad Dynamic Range (2.73-22.23) mg/L as well as a Resolution of -0.01 mg/L with an accuracy of ± 4%. The calibrated FNOP was utilised for continuous measuring of oxygen concentration gradient for cell lines RIN-m5F / HeLa for more than five days in alginate hydrogel spheres *in vitro*.

Keywords: Bio Sensors, Fluorescence, HeLa Cells, Oxygen Sensor, Optical sensors, RIN-m5F

1. Introduction:

According to the world health organization, diabetes is one of the top fifteen leading causes of death in the world for the year 2002, though it is projected to be in 7th position by 2030 [1], but currently in 6th position and accounted for approximately 1.6 million deaths in 2015. There was approximately a 50% increase in death due to diabetes from 2000 to 2012. This disease still urgently requires medical therapies to tackle the fatalities and to deliver cost effective strategies for the detection and treatment of the disease. It is necessary to develop techniques which can detect, monitor and cure the disease. Currently, there are a number of technologies which can help to tackle the effects of diabetes and the development of bio-artificial pancreas is one strategy with promise by providing insulin production and release [2].

To produce a bio artificial pancreas, Beta cells are encapsulated in biocompatible material, cultured *in vitro* and then injected into patients [3]. Theoretically the cells in the encapsulated material will respond accordingly to the glucose level [4]. A major limiting factor in the development of the artificial pancreas is the optimization of encapsulation. The encapsulation material must defend the cells within from the host immune response, allow the release of exogenous factors produced by the encapsulated cells, and provide for the necessary mass transport exchange of nutrients, oxygen and other factors that are essential to maintain the encapsulated cells [5, 6]. Therefore, the material must act as a selectively permeable barrier. The size and composition of the encapsulating material or hydrogel is also a critical factor in the performance of the artificial pancreas.

Cell encapsulation techniques give a greater flexibility in dynamic sizes but sizes greater than 0.1 mm seriously suffers from depletion of the oxygen and nutrient diffusion during pre and post-transplantation. The volume of cells is majorly determined by the size of hydrogel and diffusion of nutrients, and immunological responses. In the work by Vegas, A. J et.al [7], the sizes of alginate spheres were varied in the range of 0.5 mm to 1.5 mm and it was observed that the 1.5 mm modified alginate spheres were advantageous in terms of reducing immunological responses when compared to 0.5 mm sized spheres. However, the oxygen distribution across the larger sphere varied with few cells remaining inside the center of the sphere. In this research the oxygen distribution within spheres has been evaluated, this could potentially aid in designing of the spatial and temporal controlling of in-situ oxygen generating biomaterials which can be employed inside the encapsulated materials to prolong cell viability. [8-11]

Primary human derived donor cell encapsulations have proven efficacy in terms of diabetes control, there is a shortage of donor cells for socioeconomic reasons. To address this issue of a shortage of donor cells, some groups are encapsulating embryonic stem cells in hydrogels, and differentiating the cells.[12] The physiological balance of oxygen, pH, and glucose levels in and around the hydrogel are key parameters in controlling the differentiation [13]. In particular, oxygen concentration plays a key role in the initial survival of encapsulated cells. [9,14,15] Deriving information regarding levels of oxygen concentration inside the material in a high spatial and temporal distribution will permit the synthesis of new material systems where cell growth and performance can be enhanced.[16] Potentially real time monitoring of oxygen levels can be achieved by fluorescent technologies.

The first oxygen sensing mechanism by fluorescence was demonstrated by Kautsky in the early 20th century [17], the first fluorescence system with an integrated UV source was developed in 1968 by Bergman. [18] A wide variety of fluorophores [19] like organic probes, metal-ligand complexes, and luminescent nanomaterials make this technique versatile. Metal-ligand complexes have a longer lifetime, and large stoke shift and are more stable when compared to organic probes. In metal-ligand complexes, Ruthenium-based oxygen sensing is the most studied and widely used fluorophore because of its wideband excitation (400-480 nm) and large stoke shift, resulting in an emission region of >610 nm. The importance and working principle of the fluorescent responsive ruthenium dye were explained by Mills. A and M.P. Coogan et al [20-24]. When a fluorophore is illuminated with a suitable wavelength, it will be excited to higher energy state S_1 from lower energy state S_0, and the relaxation path from the higher energy state to lower ground state can be possible either by fluorescence or phosphorescence (Fig. S1a). Fluorescence is a relatively faster phenomenon as compared with the phosphorescence due to spontaneous emission of energy from S_1 to S_0. If it chooses the non-radiative path from S_1 to Triplet state T_1 results in the slower decay of the process to reach ground state S_0. During this time interval, quenchers like molecular oxygen can involve in phosphorescence emission of the fluorophore. The process of quenching of the excited fluorophore in the triplet state by molecular oxygen can be one of the three different possible pathways and they are Energy transfer, Electron Transfer, and simple physical deactivation. For the transition metal complexes like ruthenium, energy transfer mechanism is the most possible mechanism because and it is dominated by the molecular collision thus limited by the diffusion of the quencher and is given by the Stern Volmer relation. [14]

Based upon data derived from previous reports a hydrophobic fluorophore of the ruthenium-based metal-ligand complex was selected for our sensing application. To avoid the photo-bleaching effect of the fluorophore, a suitable substrate material has to be chosen and this provided broad adaptability to the specific needs [25]. A fluorophore can be tethered or encapsulated onto a substrate material [26] and it can be in the form of a thin film or particle.

Within this paper, data is presented which provides evidence that the particle-based approach can provide spatiometric concentration gradient information from inside an encapsulated material for 3D tissue culture applications. The advancement of nanomaterial technology and their application in biocompatibility has huge potential in optimizing the design and of substrate materials and controlled culture conditions to induce specific forms of cell responses. [27, 28]

Previous work has successfully demonstrated the encapsulation of fluorophores in a nanoparticle for intracellular imaging [29], but very few works utilized these sensors for material optimization, via monitoring of selected parameters within a hydrogel environment that provides real time information regarding optimal environmental conditions that are required to ensure efficient cell function [8]. Previous studies have utilized commercial sensors [30-33] which are not suitable for the new generation of additive manufacturing techniques due to their large feature size of sensors which may affect toxicity and biocompatibility for a wide range of cellular phenotypes [34]. To address these issues small feature Oxygen sensors, with easy calibration, and reduced photo bleaching must be designed and tested. The objective of this research was to fabricate nanoparticles that have the ability to sense a range of oxygen concentrations by binding optical responsive fluorophores on to them and employing these sensors in 3Dimensional cellular conditions. Different concentrations of calcium and strontium gelated alginate spheres were utilised as the cell carrier and the hydrogel sizes were in the range 700-1000 μm in diameter.

2. Materials and Methods:

2.1 Materials and Reagents

Polystyrene Nano beads with surface modified by carboxyl groups (Thermo SCI-ENTIFIC, W050C), Pluronic F127, (3-Aminopropyl) triethoxysilane, Strontium chloride, Calcium chloride dehydrate, Alginic acid sodium salt (Sigma Aldrich), $Ru(dpp)_3Cl_2$ ($C_{72}H_{48}Cl_2N_6Ru$) (Fluka) (

excitation at 470-490 nm and emission at 613 nm), HeLa cell lines, RIN-mF5 cells lines, Culture well gaskets (Grace Bio Labs), Cell culture Media Gibco™ RPMI 1640 Medium 1x, Gibco™ DMEM 1x ,SPL life science culture flask, Hamilton syringe (25 μL), KD scientific syringe pump, Nitrogen and Oxygen gas cylinders (10 L), Oxygen meter (Hanna Instruments 98193), KUBOTA centrifuge 3700, MIKRO 200R centrifuge, SPELL MAN voltage controller (9 W, 30 kV | CZE1000R), JEOL JSM 6610 SEM, Zeiss LSM 780 Confocal Microscope - Inverted Microscope were employed in this study.

2.2.1 Synthesis of Functional Nano Oxygen Particles

FNOPs were fabricated using the process in Fig. 1A. 0.5mL (100mg/mL) Polystyrene Bead (PSB) solution was centrifuged at 8000 rpm for 10 minutes to extract the PSBs from the Sodium azide solution. To obtain pure PSBs a purification step was repeated in twice, DI water was mixed with PSBs and centrifuged at 8000 rpm for 10 minutes, and the supernatant was removed as well as the samples were mixed with DI water and centrifuged for a second time. The supernatant was removed and DI water was added to make a final solution of 1mL PSB solution. Pluronic F127 (0.1g/1mL of PSB) (a triblock copolymer), poly (propylene oxide) (a central hydrophobic polymer), and poly (ethylene glycol) (PEG, hydrophilic ends) were employed and attached to the surface of PSB by an esterification process, 1 mg of Oxygen-sensitive red fluorescent molecule $Ru(dpp)_3Cl_2$, ($C_{72}H_{48}Cl_2N_6Ru$) (Fluka, excitation at 470-490 nm and emission at 613 nm), dissolved in 200 μL of 99.5 % pure ethanol. The ethanol containing fluorophore solution was added to the previously prepared 1 mL solution of F127 grafted PSB and ultra-sonicated for at least 30 minutes to form functional FNOPs by hydrophobic interaction. [35] Functional FNOP particles were washed with sterile DI water by centrifuging the sample at 8000 rpm for 10 minutes, the supernatant was removed. Finally, 1mL of sterile DI water was added to the washed FNOP. The final Functional FNOPs were stored in a dark and dry place at room temperature for further experiments. To ensure spatiometric dispersion of particles throughout the suspension and to avoid aggregation because of electrostatic effects a centrifugation of FNOP stock solution at low speed of 1100 rpm for ten minutes was introduced prior to use in calibration and sensing experiments. Nanoparticles were visualized using Scanning Electron Microscopy (Fig. 1B and C). The corresponding FTIR image (Fig. 1D), suggested that the room temperature esterification process for two hours was successful in attaching PSB particles with Pluronic F127 and corresponding fluorescence image (Fig. 1E) of functional Nano oxygen particles with excitation of 470 nm and emission >610 nm.

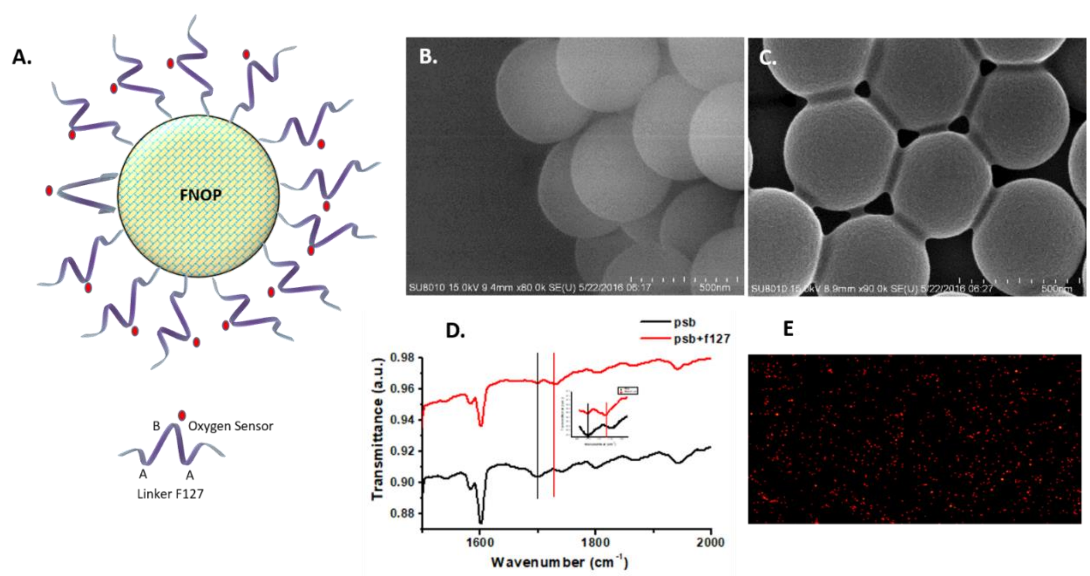

Figure 1. (A) Schematic illustration of FNOP (B) SEM image of PSBs after surface modified with carboxylic functional group. (C) SEM image of PSBs after F127 grafted. (D) Comparison of FTIR Transmission spectrum of B and C (E) Fluorescence image of FNOPs

2.2.2 Hydrogel Preparation

2.2.2. A Preparation of alginate solution

A sterilized 5 wt. % alginate solution was prepared using Alginic acid mixed with DI water on a magnetic stirrer for 12 hours at 50^0C. The prepared solution was kept for sterilization in an autoclave and stored in 4^0C until required. The hydrogels 5wt. % alginate was mixed with filtered culture media to make a 3 wt. % solution.

2.2.2. B Electrospray technique

The hydrogel spheres were prepared using electrospray technique [36]. Sterilized alginate solution was loaded into a Hamilton syringe (25µL) (Fig. 2A). The positive terminal of a high voltage power supply (5-7KV) (SPELL MAN voltage controller) was connected to the needle of the syringe and the ground terminal was applied to a metal container loaded with either Strontium chloride (0.1M $SrCl_2$) or Calcium chloride (0.1M $CaCl_2$) for the polymerization of alginate (concentrations optimized based on data derived from experiments described in section 2.2.7). The polymerized alginate hydrogel spheres were collected and further used for calibration and validation experiments. The hydrogel spheres were imaged with a confocal microscope and the structure of half spheroid and the sensor distribution inside hydrogel (Fig. 2B) which was taken with the aid of confocal microscope with a total z-axis of 400 µm in step size of 6 µm.

Equipment was sterilized by spraying 70% ethanol and kept under UV irradiation for at least 2 hours before the experiment. For measuring the oxygen concentration within cellular environments, the 3 wt. % alginate was mixed with the RIN-m5F/ HeLa cell lines in a concentration of 2.00×10^6 (cells/ mL) / 5.00×10^6 (cells/ mL) for further generation and testing of hydrogels. A MOXI Z Mini Automated Cell Counter Kit, US Version was used in measuring cellular concentration. In 1mL final volume of PBS washed trypsinzed cell a 75µL of cell solution is loaded onto the cell counting cassette and corresponding cellular concentrations were noted.

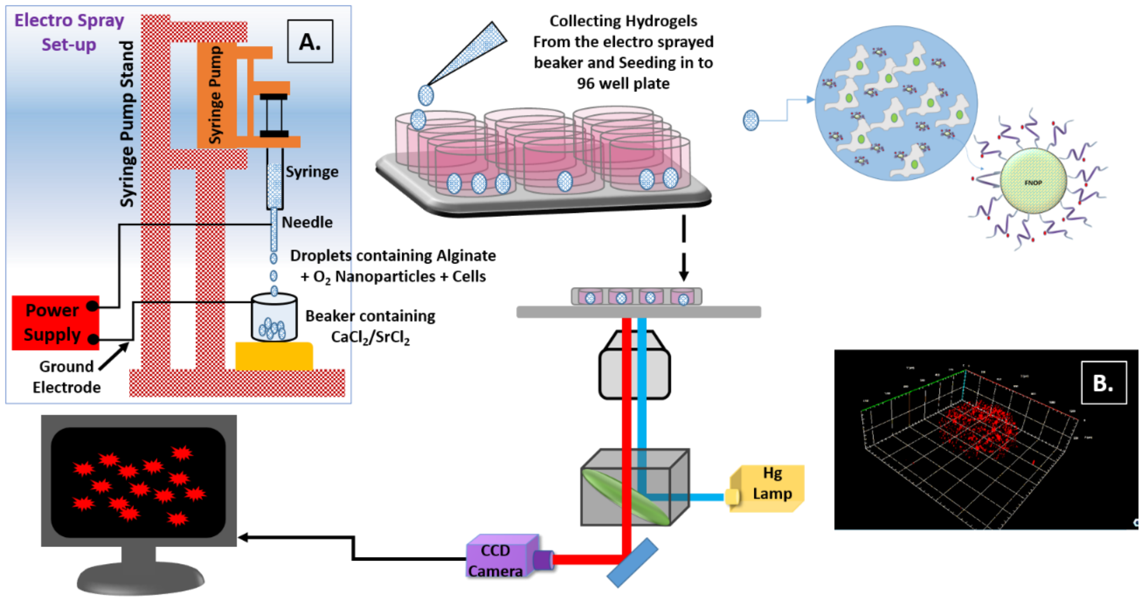

Figure (2A) Electrospray technique in generating hydrogels (2B). Confocal imaging of generated hydrogels with FNOP sensor.

2.2.3 Calibration of oxygen

A glass container filled with DI water was used for calibration, as shown in Fig. S1B. The containers contain 3 inlets for input of oxygen and nitrogen gases, as well as inserting the oxygen meter (Hanna Instruments 98193) which was used to monitor dissolved oxygen. One gas outlet was fitted with the rubber lid for free flow of gases into the chamber [37].

For calibration of oxygen in a hydrogel sphere, the alginate solution was mixed with 10 to 20 µL of FNOPs and stirred for 5 minutes using a magnetic stirrer and then the hydrogels of size ~750 µm were generated by using the technique as specified in section 2.2.2.B. The generated hydrogels were collected and pipetted evenly on to the well gasket filled with alginate. The glass slide with alginate hydrogels was placed in the water-filled container and monitored under the microscope.

For calibration in DI water, the FNOP particles were pipetted onto a modified glass substrate with the 3-Aminopropyltrimethoxy silane treated and attachment of PSBs were done by attachment of leftover carboxylic acid group on PSB to the amine functional group forming the amide bond.

2.2.4 Cell Culture

All cultures were maintained in 5% CO_2, 95% air, and at 37^0C

2.2.4. A HeLa cell lines

HeLa cell lines, were purchased from Bio resource Collection and Research Center (BCRC) and grown media consisting with Gibco™ DMEM 1x with 10% foetal bovine serum (FBS) (GIBCO), 1% penicillin – streptomycin (AppliChem).

2.2.4 B RIN-m5F cell culture

RIN-m5F cell lines, an islet beta cell, was purchased from Bio resource Collection and Research Center (BCRC) and grown media consisting with Gibco™ RPMI 1640 Medium 1x, 10% foetal bovine serum (FBS) (GIBCO), 1% L glutamine (200 mM Solution, GIBCO), 1% penicillin – streptomycin (AppliChem).

2.2.4 C Cell staining

2.2.4 C.A Hoechst

5µg/mL of Hoechst was dissolved in PBS solution and for each cell culture flask 2mL stain suspension was added and incubated for 30 minutes. The stained cell flasks were washed with PBS to remove unbounded Hoechst. Hoechst labelled cells were trypsinzed and resuspended into the appropriate concentrations for incorporation into the hydrogel experiments. RIN-m5F stained with Hoechst (Fig. S2A).

2.2.4. C.B Calcein AM Viability Stain

In initial experiments, before the encapsulation of cells into hydrogels, cells were stained with Hoechst, Hoechst intensity could not accurately determine cell viability, as the intensity decreased with time (Fig. S3) and detection of the Hoechst signal is compromised by background staining and noise, (Fig. S4). To analyze cellular viability, Calcein AM was used at regular intervals, using a batch processing technique for cellular viability in RIN-mF5 cells in hydrogels. A 1μL of Calcein AM stock solution (1μg/1μL) was dissolved in 1mL of FBS free medium and 200 μL of the dissolved or working solution was taken and used in a batch process by adding into each well of a 96 well plate. Insulin cells stained with Calcein AM in 10 mL T75 flask (Fig. S2B).

2.2.5 Toxicity

The FNOP particles were characterized for toxicity, with a varied concentration range (10μL/mL to 50μL/mL in a step size of 10μL/mL) of Nanoparticles were cultured in contact with 1.14×10^5 Hela cells in 10 mL T25 flask for 8 days and obtained the optimized concentration of 10-20μL of FNOPs as shown in Fig. S5.

2.2.6 Analysis

2.2.6 A. Image processing

The fluorescence intensities of the FNOPs were acquired by a camera through an optical microscope (OM) with the help of Cam-ware and analyzed by image software (ImageJ). The colour images were converted into 32 bit black and white images.

With the aid of Calcein AM staining, the cellular density inside the hydrogel was calculated. This was achieved by subtracting the background from the positive colour cellular images (positive Calcein stain) and then converting the images to grayscale. Threshold levels were adjusted for images to separate the background pixel intensity from the foreground pixel intensity and the number of the particles with suitable pixel size (within the size of cells) was turned in to a binary image, measured and plotted.

2.2.6 B. Statistical Analysis

To measure the oxygen concentration, an average of 10 FNOP intensities were analyzed for every hydrogel image. To measure a cellular density, 3 hydrogels stained with Calcein AM were analysed and the average value was used as the reference value, and corresponding standard deviation values were plotted as error bars. For curve fitting processes in analyzing graphs, the origin was used.

2.2.7 Hydrogel as a scaffold

To evaluate the effect of different concentrations and type of gelling agents on cell viability a series of screening experiments were conducted. RIN-m5F cells (Fig. S6A) and HeLa cells (Fig. S6B) were cultured in contact with the five different hydrogel test conditions by seeding 1.0×106 cells per well in a 6 well plate, 3wt. % alginate solution, 100mM Calcium chloride, 100mM strontium chloride solution and alginate (3wt. %) solution was gelated with Calcium chloride and Strontium chloride to form a thick substrate. In optimizing the molar concentration of $CaCl_2$ and $SrCl_2$ a range (10mM to 450mM) with a step size of 50mM were tested and better gelation was observed at 100mM concentration, this was used for optimized electrospray generation of hydrogels.

In Fig. S6A, RIN-m5F cells were cultured for 7 days without any media change, this provided for the observation of cells under the control label (cells with media) were showing a feature of floating (from 60 hours) which is a characteristic nature of Insulin cell. Though the concentration (100mM) of calcium chloride and strontium chloride was high, however after generating hydrogels, the hydrogels were washed for 3 times with the respective culture medium to ensure that leftover calcium or strontium ions should not affect the cells in hydrogels. The thin film approach of 3wt. % alginate solution cured with calcium and strontium ions (Fig. S6A) clearly shows good growth of cells. The calcium gelated alginate scaffold substrate demonstrated more effective growth of RIN-m5F cells when compared to strontium gelated alginate within a thin film structure (Fig. S6A). Though the control experiments showed some progressive results in the approach to optimizing the hydrogel-based approach for the RIN-m5F cell culture. The parameters obtained cannot be completely relied on from this approach to be applied further for the 3D spheroid model, because the structural and environmental conditions differed 2D model to 3D model.

2.2.8 SEM sample preparation

For imaging the FNOP sensors, the sensors were pipetted onto the Silicon wafer and then dried under room temperature, coated with chromium, for about 10 to 15 nm for visualization under SEM. For imaging the hydrogels, alginate was pipetted onto the glass slide and then gelated with calcium and strontium ions. The gelated hydrogels were dried under room temperature and the dried sample was placed onto sample holder with the aid of carbon tape and coated with chromium for about 10 to 15 nm for visualization under SEM.

Results and Discussion:

The optimized FNOP/cell concentration was used to assess the effect of culturing FNOPs in contact with RIN-m5 cells and no toxic effect was observed. Results from this initial study also demonstrated that FNOPs were able to enter inside or attach to the HeLa cells whereas no observable FNOP particles were inside the Insulin cells (Fig. S7).

As specified in section 2.2.3 and 2.2.6 the calibration of oxygen was carried out inside the hydrogel (Fig. 3A, B, and C) and in DI water (Fig. S1C). The calibrations inside hydrogels were performed at 17^0C which was different from the room temperature, this was due to purging nitrogen gas into the chamber which decreased the water temperature (measured with temperature sensor embedded in the oxygen meter). The oxygen concentration was varied and obtained a measurable range of 2.73-22.23 mg/L, Percentage of oxygen saturation was correlated to the dissolved oxygen (DO) in mg/L by multiplying a factor of 0.69 in measuring DO levels at 37^0C, which is approximated by using Winkler method In DI water the synthesized FNOPs showed good approximation to the characteristic nature of Stern Volmer relation [14]. In addition to the calibration, the FNOP particles were observed in the hydrogel environment for 7 days and the intensity of calibration was measured at regular interval (Fig. 3D). The hydrogels were maintained in the same culture environment as standard cell culture. The curve clearly showed that there was no significant deviation in the intensity of FNOPs. This suggests that there was negligible photo bleaching. To minimize the effect of saturation of pixel intensity, the camera exposure time was optimized to 1 sec exposure as it had the least photo bleaching effect when compared to 2, 3, 4 and 5 sec camera exposure time.

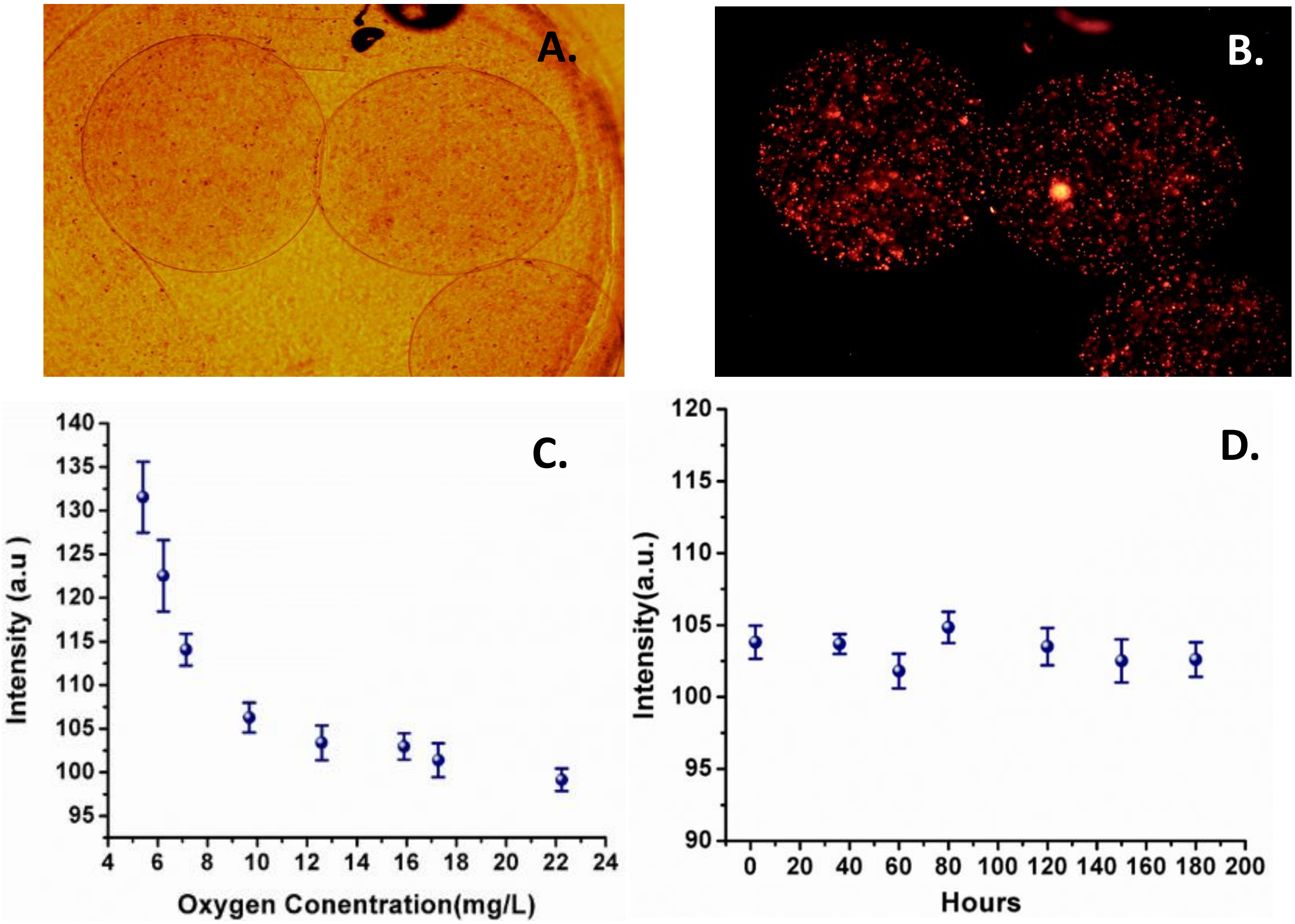

Figure (3A). Bright field view Hydrogel (3B). Fluorescence intensity of FB-FNOP at particular oxygen concentration (3C). Calibrated curve for different oxygen concentrations (3D). Intensity vs Number of hours for photo bleaching effect [Scale bar-200 μm]

Each hydrogel was generated with 700-800 RIN-m5F cells by considering 2.00×10^6 cells/ mL in alginate solution. The generated hydrogels were collected using pipette tips and were distributed evenly in the 96 well plate culture chamber, incubated at 37^0C, 5 % CO_2 and were monitored. The fluorescent image for sensing oxygen and RIN-m5F cellular viability was taken at respective time intervals (Fig. 4.A, B, and C).

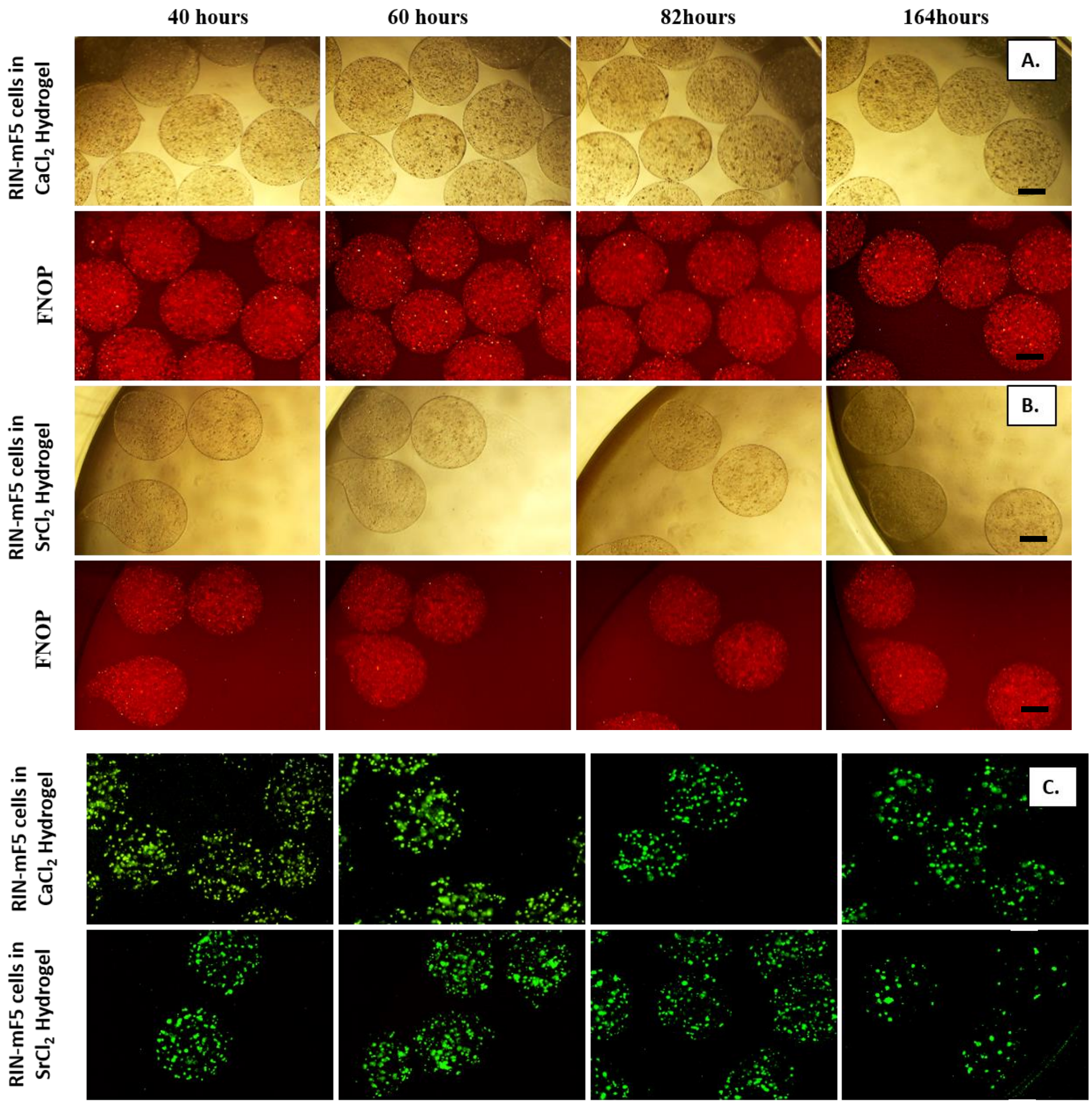

Figure (4A) Culturing of RIN-m5F in $CaCl_2$ gelated Hydrogel Red colour indicated the FNOP (4B). Culturing of RIN-m5F in $SrCl_2$ gelated Hydrogel Red colour indicated the FNOP (4C). $CaCl_2$ (Top) and $SrCl_2$ (bottom) gelated Hydrogel environment of RIN-m5F stained with Calcein AM. [Scale bar-350 µm]

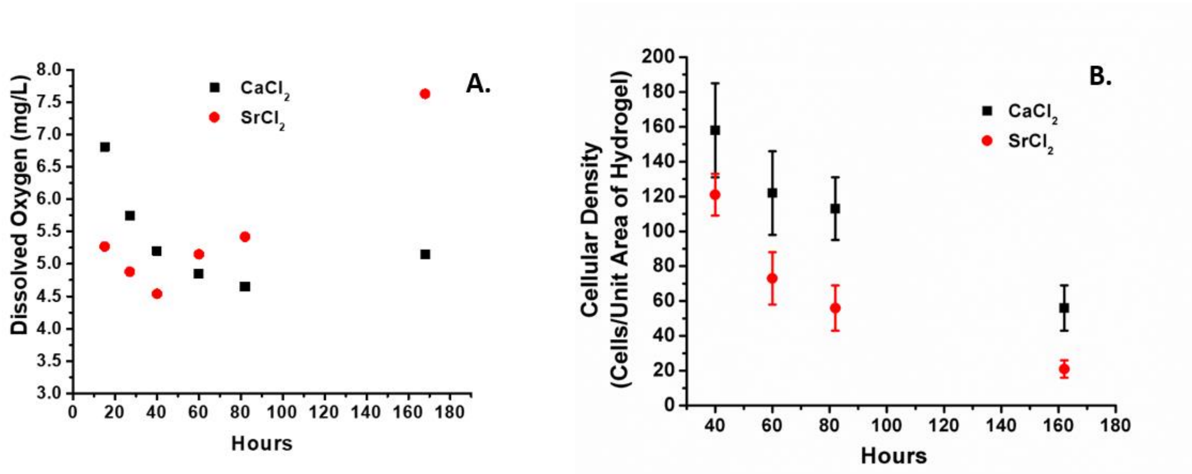

Figure (5A). Oxygen gradient in $SrCl_2$ and $CaCl_2$ gelated Hydrogel environment of RIN-m5F cells (5B) Cellular density of $CaCl_2$ and$SrCl_2$ gelated Hydrogel environment of RIN-m5F stained with Calcein AM

Fig. 5A shows the amount of oxygen inside the hydrogel at particular time intervals, the oxygen levels within hydrogel were measured by using a reference calibration and shows a behaviour of a negative gradient (consumption of oxygen by cells) till one particular time instance and then reverse its gradient. This behaviour is correlated with the cellular density which is shown in fig. 5B, which exhibits exponential decay in cellular density with time. By using a mathematical curve fitting technique, a time constant (t_1: 1/e of maximum cellular density), the change in the slope of the curve for $CaCl_2$ and $SrCl_2$ were calculated and is approximately 120 hours and 45 hours respectively. For $SrCl_2$ (Figure 5A and B), at a time instance 170 hour is approximately 4 time constants (4 t_1: 1 / [e^4]; i.e. 1.83 percent of maximum cellular density) slowly approaching to the maximum dissolved oxygen level that can be attained in the hydrogel (less oxygen consumption by cells). The same phenomenon of oxygen gradient reversal was observed in the $CaCl_2$ environment with the approximate time constant of 120 hours (t_1).

.

From the Fig. 4C, 5A and 5B, it was observed that RIN-m5 cells were enhanced viability in calcium-based hydrogels when compared to Strontium based hydrogels. Within the hydrogels, the exterior parts had greater viability compared to the interior parts or necrotic parts, this was due to the oxygen gradient in the $CaCl_2$ hydrogel environment of RIN-m5 being nearly an inverse square to the radial distance.

In a report by Komatsu, Hirotake, et al. [31] suggested that cluster of islets cells of size greater than 250 µm is highly dependent on oxygen tension and further observed that hyperoxia conditions will enhance viability, a phenomenon that is observed from figure 5A. Data shows that near hypoxic region in $SrCl_2$ resulted in greater reduction of cellular health compared to normoxia region in $CaCl_2$.

For insulin cells, the normalized intensity levels, in a $CaCl_2$ gelation hydrogel were divided into three regions (Centre, Interior, and Exterior), the corresponding intensity was plotted with time (Fig. 6) Oxygen concentration was inversely proportional to intensity. By correlating the Initial normalized average intensity with Oxygen a difference of approximately 1.22 mg/L and 0.61 mg/L was observed with the exterior region and interior respectively with a centre region, and difference of 0.54 mg/L was observed between interior and exterior regions.

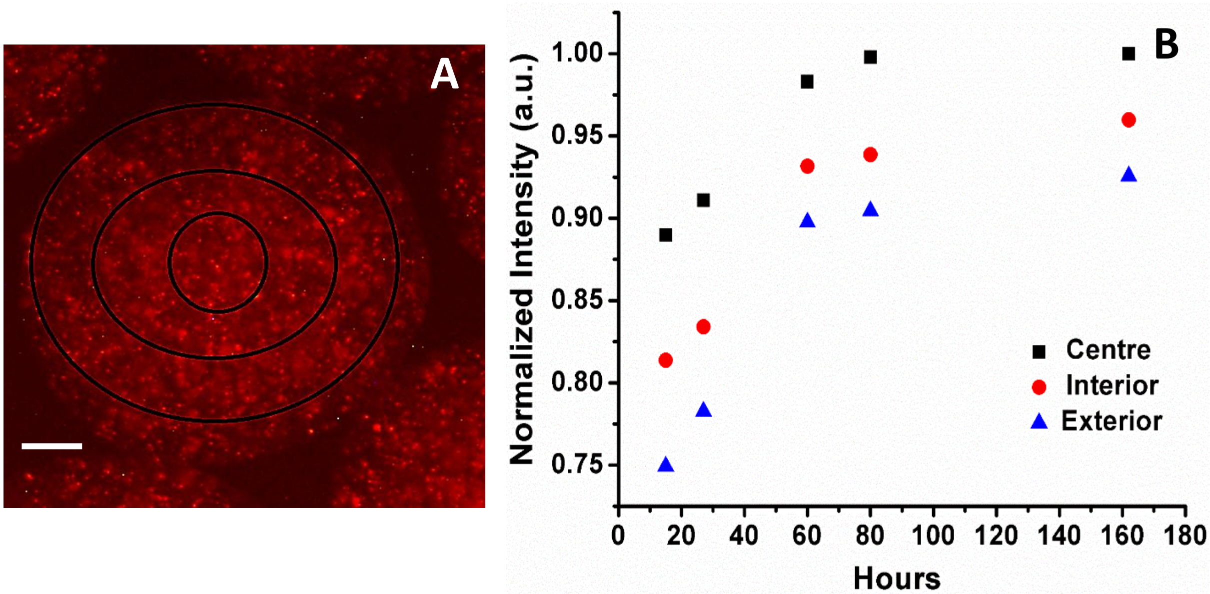

Figure (6A). FNOP distribution in centre, interior and exterior parts [Scale bar-100 μm] (6B). Normalized intensity inside RIN-m5F in one plane of Hydrogel

For Hela cells inside the 3D hydrogel environment, the gradient of oxygen with time (Fig. S4) is approximated with O_2 $CaCl_2$ (mg/L) $= 8.71 * (e^{\left(\frac{-t}{1.93}\right)}) + 3.10$, O_2 $SrCl_2$ (mg/L) $= 6.36 * (e^{\left(\frac{-t}{1.32}\right)}) + 2.50$ this showed similar exponential decay but differed in the initial level of oxygen concentration with 2.95 mg/L. As a function of time, the difference in hydrogel oxygen gradient follows a linear curve with a negative slope of 0.68 mg/L.

A confocal image at 84 hours of HeLa cellular hydrogel environment is shown in Fig. 7, the plot showed the normalized gradient of oxygen concentration for $CaCl_2$ and $SrCl_2$ gelated hydrogels from the exterior (~0 μm) to centre (~350 μm) of the hydrogel. The gradient followed the sigmoidal curve $A_2 + (A_1 - A_2)/(1 + e^{\left(\frac{x-x_0}{dx}\right)})$ in both the hydrogels, and respective values with standard deviation were shown in Table 1. The strontium gelated hydrogel exhibited a wide range of uniform values and it reached half the value at 295.38± 4.91 μm within the range for the calcium gelated hydrogel which reached 169.04 ±1.71 μm. A slope of -2.1(a.u. /mm) and -1.5

(a.u. /mm) was observed in $SrCl_2$ and $CaCl_2$ hydrogels. The diffusion coefficient of oxygen in HeLa cells incubated in hydrogel was calculated by using the Fick's law of diffusion equation in considering the rate of time equation and concentration gradient and it was found to be 1.3 * 10^{-9} m^2/sec, which is in the range of the nominal value inside polymeric hydrogels. [38-44]

The Oxygen (based on normalized intensity) spatial distribution of $CaCl_2$ and $SrCl_2$ hydrogels (Fig. S8) (generated by pipetting and imaged) demonstrated there was not a large difference in spatial difference in $CaCl_2$ hydrogel with and without cells, while the in $SrCl_2$ (Fig. 7B) showed the slow decrease of the oxygen gradient inside hydrogels, up to 250 μm from the exterior, which suggested there were enhanced viability cells in $SrCl_2$ compared to $CaCl_2$.

In addition to the oxygen tension and size of a hydrogel, the preferential respective cellular behaviour in a hydrogel material can be attributed to the factors such as mechanical response and integrin conformational changes. A mechanical response incurred by the difference in reactivity and gel strength with the calcium and strontium ions and is according to the ratio of mannuronic acid (M) and glucuronic acid (G) of alginate [45]. The different mechanical strength of extracellular matrix results in the varied behaviour of cancer cell proliferation rate, with the higher mechanical strength of extracellular matrix resulting in relatively higher proliferation [46]. The current experiments were performed with M/G ratio of 1.56 in alginate, which results in slower gelation rate with strontium when compared to calcium. The decrease in gelation rate exhibits the higher mechanical strength and uniformed structures compared to the faster gelation rate [47, 48]. Calcium and Strontium gelated hydrogel SEM images were shown in (Fig. S9). Whereas compliant substrates [49, 50] will yield a better performance compared to stiffer substrates in insulin secretion and viability of the Beta cell. Divalent Cations shows a divergent behaviour in integrin conformation, in particular, β_1 [51,52] integrin in inulin cell and $\alpha_3\beta_1$, $\alpha_5\beta_1$ [53,54] integrin's in HeLa cells (cervical cancer) plays a very crucial role on their attachment and cellular proliferation or even apoptosis in extracellular matrix environment conditions.

By observing temporal progression and Live and Dead Cell imaging in the hydrogel environment of Insulin cells, we found that the $CaCl_2$ hydrogels showed a viable micro environment compared to $SrCl_2$, whereas for Hela cells on the basis of both temporal and spatial oxygen distribution suggested $SrCl_2$ was a more suitable environment.

In addition to the material suitability to the cellular environment, the application of these highly temporal and spatial resolved monitoring approaches will greatly enhance the design efficiency in producing suitable 3D microenvironments, particularly in additive manufacturing and for different cellular applications.

Table: 1 spatial gradient of Oxygen inside Hydrogel with respect to sigmoidal curve

Hela Cell_3.5 day [$A_2 + (A_1 - A_2)/(1 + e^{\left(\frac{x-x_0}{dx}\right)})$]				
	$CaCl_2$		$SrCl_2$	
	Value	S.D	Value	S.D
A1	1.02476	0.00457	0.99136	0.002
A2	0.6686	0.00266	0.65026	0.01702
x0	169.04171	1.71293	295.388	4.90776
dx	56.77374	1.83943	40.80	2.978

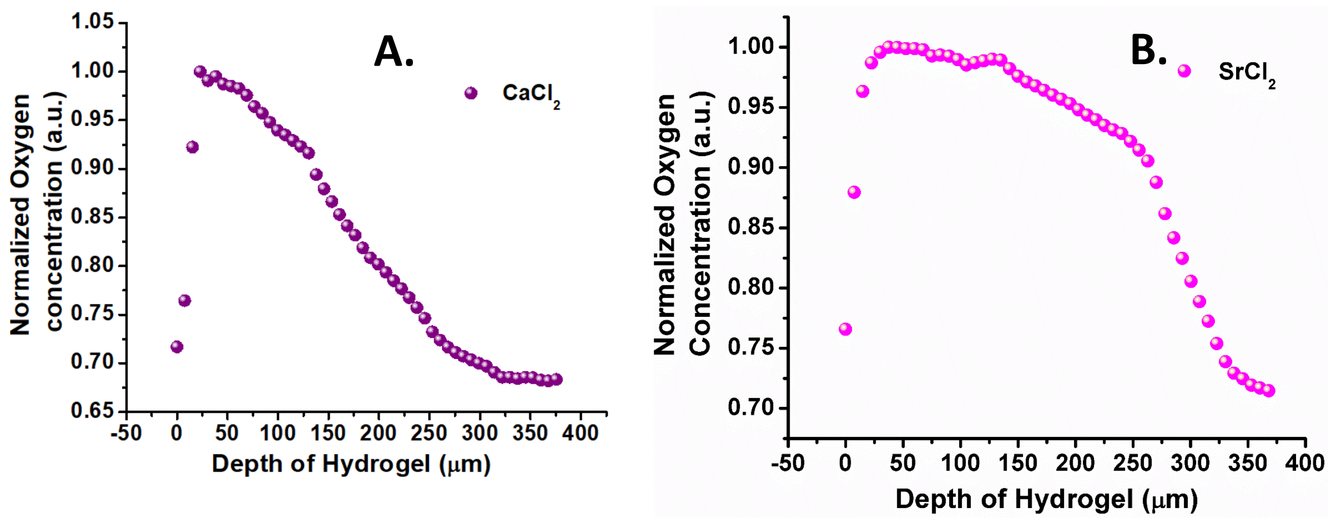

Figure.7 Oxygen gradient in $CaCl_2$ (A) and $SrCl_2$ (B) gelated Hydrogel environment of Hela Cells on 3rd day using confocal microscopy.

Conclusion:

The development of a functional nanoparticle-based oxygen sensor system that can be used to measure the oxygen concentration in 3D hydrogel tissues cultures using fluorescence microscopy has been demonstrated. RIN-m5F, and HeLa cell lines were successfully cultured with FNOPs in calcium and strontium chloride gelation hydrogel environments. In the experiments, the size of the hydrogels generated using an electrospray technique was in the range of 700-1000 μm in diameter. The oxygen concentration gradient tested the cellular viability within the calcium- and strontium- based gelation for RIN-m5F and Hela cells and demonstrated that the two different gelation ions, results in a significant difference in oxygen gradient in 3 Dimensional hydrogel environments and various suitability for different cell types. To address the need to mimic the natural environment, the fabricated FNOP sensor material with the information of high spatial and temporal distribution of oxygen should be extremely valuable in monitoring the 3D tissue material for cellular viability, which will increase the ease and rapid generation of complex and or larger hydrogel structures.

Corresponding Authors

fangang@ess.nthu.edu.tw and j.curran@liverpool.ac.uk

Acknowledgment

We would like to thanks the financial support from MOST, Taiwan by the project: MOST 103-2918-I-007-005. MOST 106-2622-E-007 -020 -CC2, MOST 106-2923-E-007-004-MY3, MOST 104-2221-E007-072-MY3, 104-2321-B-007-003, 103-2321-B-007-004, the Frontier Research Center on Fundamental and Applied Sciences of Matters (MOST107-3017-F-007-002), from The Featured Areas Research Center Program within the framework of the Higher Education Sprout Project by the Ministry of Education (MOE 107QR001I5), Taiwan and excellence university centre project for Biomedical Technology, NTHU, and 2013-2016.

Supporting Information

The Supporting Information is available free of charge on the ACS Publications website at DOI:

Schematic illustration of working principle of Oxygen sensor and Calibration in DI Water, reference Cell staining images, OM image of Cell Scaffold Experiments, Distribution of Oxygen in Hydrogels without cells.

ORCID ID

Fan Gang Tseng: 0000-0001-7654-6905
John Hunt: 0000-0002-5168-4778
Judith Curran: 0000-0003-1551-2917
James Henstock: 0000-0002-8517-0679
Manohar Koduri: 0000-0002-3760-8373

Table of Content Figure:

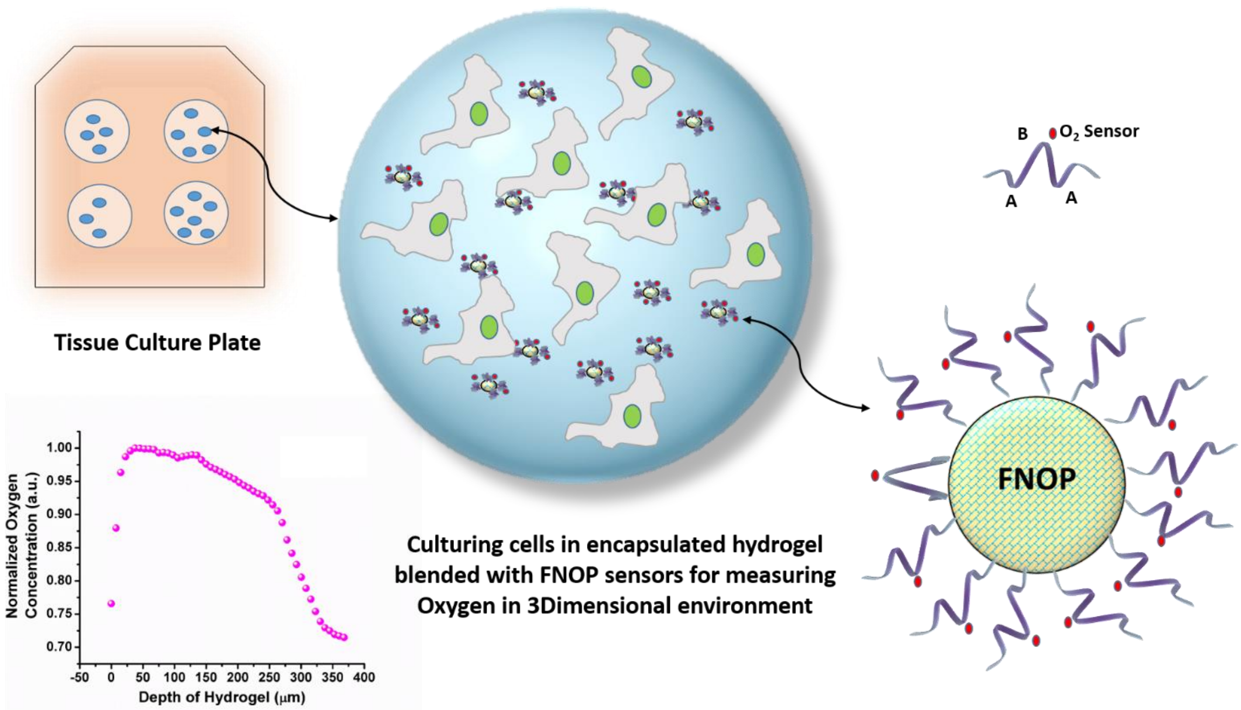

References:

(1) Mathers, C. D.; Loncar, D. Projections of Global Mortality and Burden of Disease from 2002 to 2030. PLoS medicine 2006, 3, e442.

(2) Mikos, A. G.; Papadaki, M. G.; Kouvroukoglou, S.; Ishaug, S. L.; Thomson, R. C. Mini-review: Islet Transplantation to Create a Bioartificial Pancreas. Biotechnol. Bioeng. 1994, 43, 673-677.

(3) Kobayashi, N. Bioartificial Pancreas for the Treatment of Diabetes. Cell Transplant. 2008, 17, 11-17.

(4) Pareta, R. A.; Farney, A. C.; Opara, E. C. Design of a Bioartificial Pancreas. Pathobiology 2013, 80, 194-202, DOI: 10.1159/000345873.

(5) Krishnan, R.; Alexander, M.; Robles, L.; Foster, C. E.,3rd; Lakey, J. R. Islet and Stem Cell Encapsulation for Clinical Transplantation. Rev. Diabet. Stud. 2014, 11, 84-101, DOI: 10.1900/RDS.2014.11.84.

(6) Lim, F.; Sun, A. M. Microencapsulated Islets as Bioartificial endocrine pancreas. Science 1980, 210, 908-910.

(7) Vegas, A. J.; Veiseh, O.; Gürtler, M.; Millman, J. R.; Pagliuca, F. W.; Bader, A. R.; Doloff, J. C.; Li, J.; Chen, M.; Olejnik, K. Long-term Glycemic Control using Polymer-Encapsulated Human Stem Cell–Derived Beta Cells in Immune-Competent Mice. Nat. Med. 2016, 22, 306.

(8) Desai, T.; Shea, L. D. Advances in Islet encapsulation Technologies. Nature Reviews Drug Discovery 2017, *16*, 338

(9) Lewis, D. M.; Blatchley, M. R.; Park, K. M.; Gerecht, S. O 2-Controllable Hydrogels for Studying Cellular Responses to Hypoxic Gradients in Three Dimensions in Vitro and in Vivo. Nature protocols 2017, 12, 1620.

(10) Pedraza, E.; Coronel, M. M.; Fraker, C. A.; Ricordi, C.; Stabler, C. L. Preventing Hypoxia-Induced Cell Death in Beta cells and Islets via Hydrolytically Activated, Oxygen-Generating Biomaterials. Proc. Natl. Acad. Sci. U. S. A. 2012, 109, 4245-4250, DOI: 10.1073/pnas.1113560109.

(11) Larrañaga, A.; Isa, I. L. M.; Patil, V.; Thamboo, S.; Lomora, M.; Fernández-Yague, M. A.; Sarasua, J.; Palivan, C. G.; Pandit, A. Antioxidant Functionalized Polymer Capsules to Prevent Oxidative stress. Acta biomaterialia 2018, 67, 21-31.

(12) Amer, L. D.; Mahoney, M. J.; Bryant, S. J. Tissue Engineering Approaches to Cell-Based Type 1 Diabetes Therapy. Tissue Engineering Part B: Reviews 2014, 20, 455-467.

(13) Serra, M.; Brito, C.; Correia, C.; Alves, P. M. Process Engineering of Human Pluripotent Stem Cells for Clinical Application. Trends Biotechnol. 2012, 30, 350-359.

(14) Wang, X.; Wolfbeis, O. S. Optical Methods for Sensing and Imaging oxygen: Materials, Spectroscopies and Applications. Chem. Soc. Rev. 2014, 43, 3666-3761.

(15) Grist, S. M.; Chrostowski, L.; Cheung, K. C. Optical Oxygen Sensors for Applications in Microfluidic Cell Culture. Sensors 2010, 10, 9286-9316.

(16) Hasan, A.; Nurunnabi, M.; Morshed, M.; Paul, A.; Polini, A.; Kuila, T.; Al Hariri, M.; Lee, Y. K.; Jaffa, A. A. Recent Advances in Application of Biosensors in Tissue Engineering. Biomed. Res. Int. 2014, 2014, 307519, DOI: 10.1155/2014/307519.

(17) Kautsky, H. Quenching of Luminescence by Oxygen. Transactions of the Faraday Society 1939, 35, 216-219.

(18) Bergman, I. Rapid-Response Atmospheric Oxygen Monitor based on Fluorescence Quenching. Nature 1968, 218, 396.

(19) Gijzeman, O.; Kaufman, F.; Porter, G. Oxygen Quenching of Aromatic Triplet States in Solution. Part 1. Journal of the Chemical Society, Faraday Transactions 2: Molecular and Chemical Physics 1973, 69, 708-720.

(20) Mills, A. Optical Oxygen Sensors. Platinum Metals Review 1997, 41, 115-127.

(21) Djurovich, P. I.; Murphy, D.; Thompson, M. E.; Hernandez, B.; Gao, R.; Hunt, P. L.; Selke, M. Cyclometalated Iridium and Platinum Complexes as Singlet Oxygen Photosensitizers: Quantum yields, Quenching Rates and Correlation with Electronic Structures. Dalton Transactions 2007, 3763-3770

(22) Quaranta, M.; Borisov, S. M.; Klimant, I. Indicators for Optical Oxygen Sensors. Bioanalytical reviews 2012, 4, 115-157.

(23) Coogan, M. P.; Gray, V. L.; Hayes, A. J.; Lloyd, S. H.; Millet, C. O.; Pope, S. J.; Lloyd, D. Probing Intracellular Oxygen by Quenched Phosphorescence Lifetimes of nanoparticles Containing Polyacrylamide-Embedded [Ru (dpp (SO 3 Na) 2) 3] Cl 2. Photochemical & photobiological sciences 2010, 9, 103-109.

(24) Quaranta, M.; Borisov, S. M.; Klimant, I. Indicators for Optical Oxygen Sensors. Bioanalytical reviews 2012, 4, 115-157.

(25) Adhikari, B.; Majumdar, S. Polymers in Sensor Applications. Progress in polymer science 2004, 29, 699-766.

(26) Li, K.; Liu, B. Polymer-Encapsulated Organic Nanoparticles for Fluorescence and Photoacoustic Imaging. Chem. Soc. Rev. 2014, 43, 6570-6597.

(27) Schmälzlin, E.; Van Dongen, J. T.; Klimant, I.; Marmodée, B.; Steup, M.; Fisahn, J.; Geigenberger, P.; Löhmannsröben, H. An Optical Multifrequency Phase-Modulation Method Using Microbeads for Measuring Intracellular Oxygen Concentrations in plants. Biophys. J. 2005, 89, 1339-1345.

(28) Schmälzlin, E.; Walz, B.; Klimant, I.; Schewe, B.; Löhmannsröben, H. Monitoring Hormone-Induced Oxygen Consumption in the Salivary Glands of the Blowfly, Calliphora vicina, by use of Luminescent Microbeads. Sensors Actuators B: Chem. 2006, 119, 251-254.

(29) Xu, H.; Aylott, J. W.; Kopelman, R. Fluorescent Nano-PEBBLE sensors designed for Intracellular Glucose Imaging. Analyst 2002, 127, 1471-1477.

(30) Benz, K.; Mollenhauer, J. Quality Assessment in 3D Cultures of Disc-Chondrocytes. BioProcess Int 2008, 6.

(31) Komatsu, H.; Kang, D.; Medrano, L.; Barriga, A.; Mendez, D.; Rawson, J.; Omori, K.; Ferreri, K.; Tai, Y.; Kandeel, F. Isolated human Islets Require Hyperoxia to

Maintain Islet mass, Metabolism, and Function. Biochem. Biophys. Res. Commun. 2016, 470, 534-538.

(32) Komatsu, H.; Cook, C.; Wang, C.; Medrano, L.; Lin, H.; Kandeel, F.; Tai, Y.; Mullen, Y. Oxygen Environment and Islet size are the Primary Limiting Factors of Isolated Pancreatic Islet survival. PloS one 2017, 12, e0183780.

(33) Figueiredo, L.; Pace, R.; D'Arros, C.; Réthoré, G.; Guicheux, J.; Le Visage, C.; Weiss, P. Assessing Glucose and Oxygen Diffusion in hydrogels for the Rational Design of 3D Stem Cell Scaffolds in Regenerative Medicine. Journal of tissue engineering and regenerative medicine 2018, 12, 1238-1246.

(34) Yan, Y.; Such, G. K.; Johnston, A. P.; Best, J. P.; Caruso, F. Engineering Particles for Therapeutic Delivery: Prospects and Challenges. ACS nano 2012, 6, 3663-3669.

(35) Khan, M. I.; Azizli, K.; Sufian, S.; Man, Z.; Khan, A. S. Simultaneous Preparation of Nano silica and Iron Oxide from Palm Oil Fuel Ash and Thermokinetics of Template Removal. RSC Advances 2015, 5, 20788-20799.

(36) Almería, B.; Gomez, A. Electrospray Synthesis of Monodisperse Polymer Particles in a Broad (60 Nm–2 Mm) Diameter Range: Guiding Principles and Formulation Recipes. J. Colloid Interface Sci. 2014, 417, 121-130.

(37) Kim, H. D.; Yi, S. J.; Kim, K. C. Simultaneous Measurement of Dissolved Oxygen Concentration and Velocity Field in Microfluidics Using Oxygen-Sensitive Particles. Microfluidics and Nanofluidics 2013, 15, 139-149.

(38) Kellner, K.; Liebsch, G.; Klimant, I.; Wolfbeis, O. S.; Blunk, T.; Schulz, M. B.; Göpferich, A. Determination of Oxygen Gradients in Engineered Tissue Using a Fluorescent Sensor. Biotechnol. Bioeng. 2002, 80, 73-83.

(39) Lesher-Pérez, S. C.; Kim, G.; Kuo, C.; Leung, B. M.; Mong, S.; Kojima, T.; Moraes, C.; Thouless, M.; Luker, G. D.; Takayama, S. Dispersible Oxygen Microsensors Map Oxygen Gradients in Three-Dimensional Cell Cultures. Biomaterials Science 2017, 5, 2106-2113.

(40) Malda, J.; Rouwkema, J.; Martens, D. E.; Le Comte, E. P.; Kooy, F.; Tramper, J.; Van Blitterswijk, C. A.; Riesle, J. Oxygen Gradients in Tissue- Engineered Pegt/Pbt Cartilaginous Constructs: Measurement and Modeling. Biotechnol. Bioeng. 2004, 86, 9-18.

(41) Mcmurtrey, R. J. Analytic Models Of Oxygen And Nutrient Diffusion, Metabolism Dynamics, and Architecture Optimization in Three-Dimensional Tissue Constructs with Applications and Insights in Cerebral Organoids. Tissue Engineering Part C: Methods 2016, 22, 221-249.

(42) Super, A.; Jaccard, N.; Marques, M. P. C.; Macown, R. J.; Griffin, L. D.; Veraitch, F. S.; Szita, N. Real- Time Monitoring of Specific Oxygen Uptake Rates of Embryonic Stem Cells in a Microfluidic Cell Culture Device. Biotechnology Journal 2016, 11, 1179-1189.

(43) Westphal, I.; Jedelhauser, C.; Liebsch, G.; Wilhelmi, A.; Aszodi, A.; Schieker, M. Oxygen Mapping: Probing a Novel Seeding Strategy for Bone Tissue Engineering. Biotechnol. Bioeng. 2017, 114, 894-902.

(44) Zhao, F.; Pathi, P.; Grayson, W.; Xing, Q.; Locke, B. R.; Ma, T. Effects of Oxygen Transport on 3- D Human Mesenchymal Stem Cell Metabolic Activity in Perfusion and Static Cultures: Experiments And Mathematical Model. Biotechnol. Prog. 2005, 21, 1269-1280.

(45) Mørch, Ý. A.; Donati, I.; Strand, B. L.; Skjåk-Bræk, G. Effect Of Ca2 , Ba2 , and Sr2 on Alginate Microbeads. Biomacromolecules 2006, 7, 1471-1480.

(46) Katira, P.; Bonnecaze, R. T.; Zaman, M. H. Modeling the Mechanics of Cancer: Effect of Changes in Cellular and Extra-Cellular Mechanical Properties. Frontiers in Oncology 2013, 3, 145.

(47) Kaklamani, G.; Cheneler, D.; Grover, L. M.; Adams, M. J.; Bowen, J. Mechanical Properties of Alginate Hydrogels Manufactured Using External Gelation. Journal of the Mechanical Behavior of Biomedical Materials 2014, 36, 135-142.

(48) Kuo, C. K.; Ma, P. X. Ionically Crosslinked Alginate Hydrogels as Scaffolds for Tissue Engineering: Part 1. Structure, Gelation Rate and Mechanical Properties. Biomaterials 2001, 22, 511-521.

(49) Nyitray, C. E.; Chavez, M. G.; Desai, T. A. Compliant 3D Microenvironment Improves Β-Cell Cluster Insulin Expression through Mechanosensing and Β-Catenin Signaling. Tissue Engineering Part A 2014, 20, 1888-1895.

(50) Vetere, A.; Wagner, B. K. Chemical Methods to Induce Beta-Cell Proliferation. International Journal of Endocrinology 2012, 2012.

(51) Smith, J. W.; Piotrowicz, R. S.; Mathis, D. A Mechanism for Divalent Cation Regulation of Beta 3-Integrins. J. Biol. Chem. 1994, 269, 960-967.

(52) Tiwari, S.; Askari, J. A.; Humphries, M. J.; Bulleid, N. J. Divalent Cations Regulate the Folding and Activation Status of Integrins During their Intracellular Trafficking. J. Cell. Sci. 2011, 124, 1672-1680. DOI: 10.1242/jcs.084483

(53) Landry, J. J.; Pyl, P. T.; Rausch, T.; Zichner, T.; Tekkedil, M. M.; Stutz, A. M.; Jauch, A.; Aiyar, R. S.; Pau, G.; Delhomme, N.; Gagneur, J.; Korbel, J. O.; Huber, W.; Steinmetz, L. M. The Genomic and Transcriptomic Landscape of a HeLa Cell Line. G3 (Bethesda) 2013, 3, 1213-1224, DOI: 10.1534/g3.113.005777.

(54) De Franceschi, N.; Hamidi, H.; Alanko, J.; Sahgal, P.; Ivaska, J. Integrin Traffic - the Update. J. Cell. Sci. 2015, 128, 839-852, DOI: 10.1242/jcs.161653.